

## Article

# Vehicle Engine Noise Cancellation Based on a Multi-Channel Fractional-Order Active Noise Control Algorithm

Tao Li <sup>1,2,3</sup>, Minqi Wang <sup>1</sup>, Yuyao He <sup>1</sup>, Ning Wang <sup>1</sup>, Jun Yang <sup>3</sup>, Rongjun Ding <sup>2</sup> and Kaihui Zhao <sup>4,5,\*</sup> <sup>1</sup> College of Railway Transportation, Hunan University of Technology, Zhuzhou 412007, China<sup>2</sup> College of Mechanical and Vehicle Engineering, Hunan University, Changsha 410083, China<sup>3</sup> Zhuzhou Times New Material Technology Co., Ltd., Zhuzhou 412007, China<sup>4</sup> College of Electrical and Information Engineering, Hunan University of Technology, Zhuzhou 412007, China<sup>5</sup> College of Engineering, Tokyo University of Technology, Hachioji, Tokyo 192-0982, Japan

\* Correspondence: zhaokaihui@hut.edu.cn

**Abstract:** For the problem of low-frequency noise suppression in a large area of the vehicle space, this paper proposes a novel multi-channel fractional-order active noise control algorithm and tests its ability for vehicle engine noise cancellation. The algorithm uses fractional-order calculus to replace the integer-order gradient descent to update the weighting coefficients of the filter, thereby avoiding imbalance or over-tuning phenomena during adaptive active noise cancellation and improving the control accuracy of the algorithm. A computer simulation was conducted in the noise cancellation scene of the vehicle, which showed that the algorithm is capable of suppressing single- and mixed-frequency noises, reducing the average sound pressure by approximately 20 dB. The experimental results demonstrated that the algorithm can effectively reduce the peak sound pressure of low-frequency noise for a certain type of vehicle engine by approximately 10 dB, whereas the total sound pressure level is reduced by approximately 4.7 dB.



**Citation:** Li, T.; Wang, M.; He, Y.; Wang, N.; Yang, J.; Ding, R.; Zhao, K. Vehicle Engine Noise Cancellation Based on a Multi-Channel Fractional-Order Active Noise Control Algorithm. *Machines* **2022**, *10*, 670. <https://doi.org/10.3390/machines10080670>

Academic Editors: Donghong Ning and Shuaishuai Sun

Received: 1 July 2022

Accepted: 2 August 2022

Published: 9 August 2022

**Publisher's Note:** MDPI stays neutral with regard to jurisdictional claims in published maps and institutional affiliations.



**Copyright:** © 2022 by the authors. Licensee MDPI, Basel, Switzerland. This article is an open access article distributed under the terms and conditions of the Creative Commons Attribution (CC BY) license (<https://creativecommons.org/licenses/by/4.0/>).

**Keywords:** active noise control; fractional-order calculus; multi-channel; variable step size; vehicle noise

## 1. Introduction

Active noise control (ANC) [1–3] technology is a specific application of computer and electronic technology in the field of noise control. It uses the principle of destructive interference between sound fields of the primary and secondary noise sources to eliminate or reduce noise by generating anti-noise waves of equal amplitude but opposite phase. Because of the extensive use of high-performance, low-cost digital signal processor chips, ANC technology has gradually become important for noise control and is widely used in earphone [4,5], automobiles [6], airplanes [7], yachts [8–10], and power transformers [11].

Survey articles on ANC techniques have been published by many researchers. Zhou proposed normalized LMS (N-LMS) algorithms [12] and their optimization algorithms. Qin proposed the Sigmoid function-based LMS (SVS-LMS) [13] algorithm. The diameter of the noise cancellation area or control zone generated by a conventional single-channel ANC algorithm (e.g., Filter-x Least Mean Square, FxLMS) is approximately one-tenth of the wavelength of the controlled noise [14], and the effective range is approximately 10–20 cm in diameter. However, this kind of small area noise reduction is far from enough for practical engineering applications. Large-area spatial vehicle noise control requires a multi-channel ANC algorithm [15–19], by which, according to the size of the target noise cancellation space, multiple microphones and speakers are used to collect and control global space noise signals. At the same time due to the complexity of a vehicle's large-area spatial sound field, the step-size factor in the conventional adaptive control algorithm has a contradiction, namely that it is difficult to simultaneously satisfy the convergence rate and convergence error. Thus, research and development of variable step-size control [20–25] have become an important optimization direction.

Research on the fractional-order calculus has developed rapidly in recent years. Compared with the integer-order calculus approach, it has unique advantages [26,27] and gained various applications in engineering. Particularly in the field of signal processing and control [28], fractional-order calculus can describe a system more accurately [29–31] and perform accurate and robust parameter estimation and iteration for nonlinear systems, achieving better results than integer-order calculus. Therefore, fractional-order algorithms [32–35] have been considered for the research in the field of ANC. Several scholars have developed ANC algorithms based on the fractional-order approach. For example, previous studies [36,37] used the fractional-order-based least mean square algorithm for the off-line identification of secondary paths to improve the accuracy of identification. Other studies [38,39] used fractional-based ANC algorithms to control specific noise (e.g., impulse noise) and good results were achieved. However, the existing research on the fractional-order-based ANC algorithms is limited to the noise signal extraction and control of specific noise or applied to secondary path identification. Only few studies have investigated the multi-channel fractional-order ANC algorithm and the application of vehicle engine noise ANC with large control area.

This paper proposes a multi-channel fractional-order ANC algorithm (MFO-FxLMS). The algorithm is characterized with an efficient description of a nonlinear system by fractional-order calculus, and the single-channel ANC method is extended to a multi-channel control method. The step size factor in the proposed algorithm is variable, resulting in reduced convergence error and hence fast convergence rate. The effect of the proposed ANC algorithm is optimized in an application scenario of vehicle engine noise cancellation with a large control area.

## 2. Multi-Channel Fractional-Order ANC Algorithm

### 2.1. Conventional ANC Algorithm

Assuming that the actual output of the system is  $y(n)$  and the expected output is  $d(n)$ , the tracking error is defined as  $e(n) = d(n) - y(n)$ . The core of the system is an FIR (finite impulse response) transversal filter (Figure 1a).

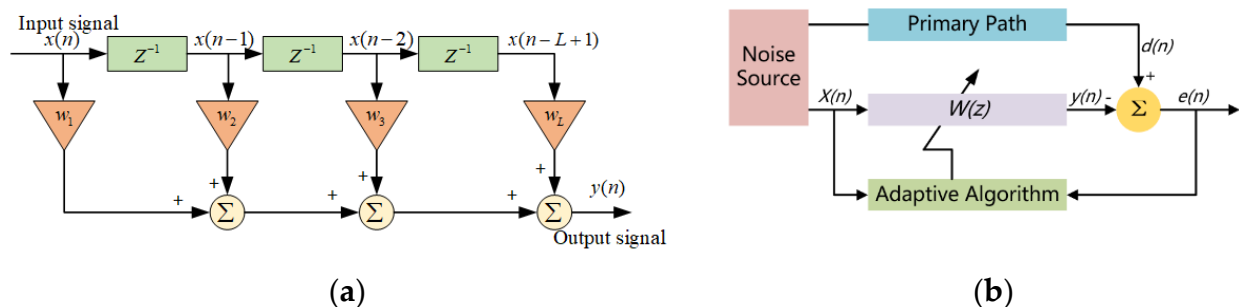


**Figure 1.** Block diagram of ANC algorithm: (a) Transversal filter; (b) ANC system.

Here,  $X(n)$  is the reference input signal obtained by the microphone acquiring the noise source, which can be expressed as  $X(n) = [x(n), x(n-1), \dots, x(n-L+1)]^T$ . The weighting coefficient vector is expressed as  $W(n) = [w_1(n), w_2(n), \dots, w_L(n)]^T$ .

The system output can be expressed as

$$y(n) = X^T(n)W(n) = \sum_{l=1}^L w_l(n)x(n-l+1) \quad (1)$$

The control system is shown in Figure 1b, and the error signal  $e(n)$  can be expressed as

$$e(n) = d(n) - y(n) = d(n) - X^T(n)W(n) \quad (2)$$

The ANC algorithm adopts the gradient descent method, and its objective function [1,2] is defined as

$$J(n) = E[e(n)^2] = E[(d(n) - y(n))^2] \quad (3)$$

where  $E[\cdot]$  is the expectation operator. Then, the filter weighting coefficient according to the specific iterative algorithm of the gradient descent method takes the form

$$W(n+1) = W(n) - \mu \nabla(n) \quad (4)$$

where  $\mu$  is the convergence step size and  $\nabla(n)$  is the reverse gradient of  $J(n)$  with respect to the weight vector  $W(n)$ . For practical applications,  $E[e(n)]^2$  can be substituted by  $e(n)^2$  for the convenience of real-time system implementation. The estimated gradient vector  $\hat{\nabla}(n)$  can be expressed as

$$\hat{\nabla}(n) = \frac{\partial e(n)^2}{\partial W} = -2e(n)X(n) \quad (5)$$

As  $E[\hat{\nabla}(n)] = \nabla(n)$ , this estimator is unbiased. Equation (4) can be expanded to

$$W(n+1) = W(n) + 2\mu e(n)X(n) \quad (6)$$

Simultaneously, the weight coefficient momentum can be introduced to increase the stability of the algorithm during convergence process. Equation (4) can be expanded to

$$W(n+1) = W(n) + 2\mu e(n)X(n) + \lambda \Delta W(n) \quad (7)$$

where  $\lambda$  is the momentum factor and  $\Delta W(n)$  is the weighted momentum, whose expression is

$$\Delta W(n) = W(n) - W(n-1) \quad (8)$$

The FxLMS algorithm is computationally simple. Its step size  $\mu$  is a fixed parameter. In order to obtain better noise reduction, variable-step active noise control (ANC) methods [40–43] were proposed. Some scholars proposed the normalized LMS (N-LMS) algorithm [12], and others proposed the Sigmoid function-based LMS (SVS-LMS) algorithm [13]. However, these algorithms are difficult to satisfy simultaneously in terms of convergence speed, tracking rate and steady-state error in a balanced manner. For the problem, a fractional-order-based ANC algorithm (Multi-channel Fractional-Order Filter-x LMS, MFO-FxLMS) is proposed to optimize the convergence parameters by constructing a time-varying function related to the amount of error signal variation. This algorithm introduces fractional-order calculus to control the update iterations of the adaptive filter weight coefficients, combining integer order with fractional-order. The algorithm uses fractional-order to improve the accuracy of the random signal description and improve the performance of the noise reduction.

## 2.2. Multi-Channel Fractional-Order ANC Algorithm

In a multi-channel ANC system, the reference input signal  $X(n)$  is matrix of  $L \times L_e$ ; there are  $L$  sub-filters in filter bank  $W$  with length  $L_e$ , and the error signal  $e(n)$  is a vector signal of  $L$  length. The primary sound source is  $P(n)$ , and the primary path from the primary sound source to the target area is represented by response  $P(z)$ . The secondary path is represented by response  $H(z)$ , the estimation of the secondary path is represented by response  $\hat{H}(z)$ , and the length is  $L_h$ . The multi-channel fractional-order ANC algorithm block diagram is shown in Figure 2.

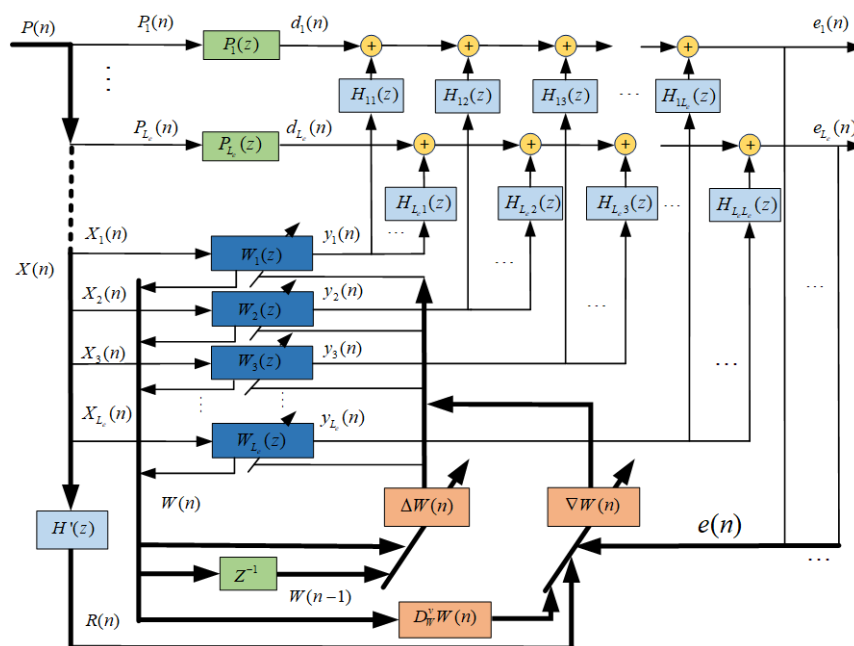


Figure 2. Block diagram of multi-channel fractional-order ANC algorithm.

For the whole system, there are

$$y_{l_e}(n) = W_{l_e}^T(n) X_{l_e}(n) \tag{9}$$

The error signal  $e(n)$  can be expressed as

$$e_{l_e}(n) = d_{l_e}(n) + \sum_j^{L_e} \sum_l^{L_h} h_{l_ej}(l) y_j(n-l+1) \tag{10}$$

where  $d_{l_e}(n)$  is the expected signal, generated by the primary sound source  $P_{l_e}(n)$  shown in Figure 2 through primary path response  $P_{l_e}(z)$ ,  $W_{l_e}(n)$  is the vector of  $L$ -order control filter coefficients, and  $R_{l_e}(n)$  is the  $L \times L_e$  matrix of the filtered- $x$  signal, formed by filtering reference input signal  $X_{l_e}(n)$  through response model  $H'(z)$ :

$$R(n) = \begin{bmatrix} R_1(n) \\ R_2(n) \\ \vdots \\ R_{L_e}(n) \end{bmatrix} = \begin{bmatrix} r_1(n)r_1(n-1) \cdots r_1(n-L+1) \\ r_2(n)r_2(n-1) \cdots r_2(n-L+1) \\ \vdots \\ r_{l_e}(n)r_{l_e}(n-1) \cdots r_{l_e}(n-L+1) \end{bmatrix} \tag{11}$$

Among which

$$r_{l_e}(n) = \sum_{l=1}^{L_h} h'_{l_e}(l) x_{l_e}(n-l+1) \tag{12}$$

where  $h'_{l_e}$  is the filter coefficient vector of the FIR filter, which simulates the device response from the  $l_e^{th}$  controller to the error sensor, and  $x_{l_e}$  is the vector of the  $l_e^{th}$  reference signal in the previous sampling period. The  $L_e$  dimensional vector of the control filter coefficient in Equation (9) is constructed as

$$W(n) = [W_1^T(n) \ W_2^T(n) \ W_3^T(n) \ \cdots \ W_{L_e}^T(n)] \tag{13}$$

Among which,  $W_{l_e}(n)$  is the  $L_e$  dimensional coefficient vector, expressed as

$$W_{l_e}(n) = [W_{1l_e}^T(n) \ W_{2l_e}^T(n) \ W_{3l_e}^T(n) \ \cdots \ W_{L_e l_e}^T(n)] \tag{14}$$

In a multi-channel ANC system, the controller usually minimizes the objective function given by the sum of squared errors. Thus, the objective function can be written as

$$J = \frac{1}{2} \sum_{l_e=1}^{L_e} E[e_{l_e}^2(n)] \quad (15)$$

Compared with the conventional ANC algorithm, the filter weight coefficients are updated using the fractional-order calculus. The reverse gradient  $\nabla W(n)$  calculation process is as follows:

$$\nabla W(n) = \left. \frac{\partial^v J}{\partial W^v} \right|_{W=W(n)} = \frac{\partial^v \frac{1}{2} [e(n)]^2}{\partial W^v} = e(n) \frac{\partial^v e(n)}{\partial W^v} = e(n) D_W^v [e(n)] \quad (16)$$

$$D_W^v [e(n)] = D_W^v [d(n) - y(n)] = D_W^v [d(n) + R(n)W(n)] = R(n) D_W^v [W(n)] \quad (17)$$

where  $D[\cdot]$  is the differential operator. The  $n$ th derivative of power function  $t^m$  [35,36] can be expressed as

$$\frac{d^n}{dt^n} t^m = m(m-1) \cdots (m-n+1) t^{m-n} = \frac{m!}{(m-n)!} t^{m-n} \quad (18)$$

Equation (18) can be directly extended to the fractional-order derivative:

$$D_t^v t^m = \frac{\Gamma(m+1)}{\Gamma(m-v+1)} t^{m-v}, m > -1 \quad (19)$$

When  $m = 1$ , Equation (17) can be written as

$$D_W^v [e(n)] = R(n) D_W^v [W(n)] = R(n) \frac{\Gamma(2)[W(n)]^{1-v}}{\Gamma(2-v)} \quad (20)$$

Substituting Equation (20) into Equation (16) yields

$$\nabla W(n) = e(n) R(n) \frac{\Gamma(2)[W(n)]^{1-v}}{\Gamma(2-v)} \quad (21)$$

Using the steepest descent method and adjusting the filter coefficients according to the iterative formula to minimize the objective function, the iterative formula can be expanded to

$$W_{l_e}(n+1) = W_{l_e}(n) - \mu e_{l_e}(n) R_{l_e}(n) \frac{\Gamma(2)[W_{l_e}(n)]^{1-v}}{\Gamma(2-v)} + \lambda [W_{l_e}(n) - W_{l_e}(n-1)] \quad (22)$$

where  $\mu$  is the convergence step size, it can be set here as a variable step size function  $\mu(n)$ , which could improve the system offset due to the nonzero convergence step size.  $\mu(n)$  is expressed as

$$\mu = \mu(n) = \frac{\Gamma(3-v)}{\Gamma(2-v)\Gamma(3)} \frac{\beta}{1 + e^{(-\alpha|e(n)-e(n-1)|)^2}} \quad (23)$$

Here,  $\beta$  is the initial step size,  $\alpha$  is the variable gain, and  $\beta > 0$  and  $\alpha > 0$ . This algorithm is named the Multi-channel Fractional-order ANC (MFO-FxLMS) algorithm in Table 1.

**Table 1.** Multi-channel fractional-order ANC (MFO-FxLMS) algorithm.

MFO-FxLMS Algorithm
$y_{l_e}(n) = W_{l_e}^T(n)X_{l_e}(n)$
$e_{l_e}(n) = d_{l_e}(n) + \sum_j^{L_e} \sum_l^{L_h} h_{l_ej}(l)y_j(n-l+1)$
$W_{l_e}(n+1) = W_{l_e}(n) - \mu(n)e_{l_e}(n)R_{l_e}(n) \frac{\Gamma(2) W_{l_e}(n) ^{1-v}}{\Gamma(2-v)} + \lambda[W_{l_e}(n) - W_{l_e}(n-1)]$
$R_{l_e}(n) = \sum_{l=1}^{L_h} h'_{l_e}(l)x_{l_e}(n-l+1)$
$\mu(n) = \frac{\Gamma(3-v)}{\Gamma(2-v)\Gamma(3)} \frac{\beta}{1+e^{(-\alpha e(n)-e(n-1) ^2)}}$

2.3. Convergence of the MFO-FxLMS Algorithm

The ANC algorithm may easily diverge when applied in the noise cancellation scene of a large area of the vehicle, so it is necessary to prove its convergence. The basic assumption is that when the iteration time tends to infinity, the global optimal solution of the system is finally found as

$$P_{dr} = E[d(n)R(n)] \tag{24}$$

$$R_{rr} = E[R(n)R^T(n)] \tag{25}$$

The objective function of the union algorithm is expressed as

$$J(n) = \frac{1}{2}[E[d^2(n)] + 2P_{dr}^T W(n) + W^T(n)R_{rr}W(n)] \tag{26}$$

According to the principle of the steepest descent method, the optimal weighting vector is obtained as

$$W_0 = -R_{rr}^{-1}P_{dr} \tag{27}$$

When the secondary path is a pure delay path, the gradient estimate value in vector iteration formula of the weighting coefficient can be set as

$$\hat{\nabla}(n) = \left. \frac{\partial^v J(n)}{\partial W^v} \right|_{W=W(n)} \tag{28}$$

Substituting Equation (26) into the Equation (28)

$$\hat{\nabla}(n) = [P_{dr} + R_{rr}W] \frac{\mu\Gamma(2)|W(n)|^{1-v}}{\Gamma(2-v)} \tag{29}$$

Therefore, the weighting vector iteration equation becomes

$$W(n+1) = W(n) - [P_{dr} + R_{rr}W] \frac{\mu\Gamma(2)|W(n)|^{1-v}}{\Gamma(2-v)} + \lambda[W(n) - W(n-1)] \tag{30}$$

Substituting Equation (27) into the Equation (30)

$$W(n+1) = W(n) - R_{rr}[W(n) - W_0] \frac{\mu\Gamma(2)|W(n)|^{1-v}}{\Gamma(2-v)} + \lambda[W(n) - W(n-1)] \tag{31}$$

As  $R_{rr}$  is the  $L \times L$  order autocorrelation matrix of the filtered- $x$  signal, which is a symmetric positive definite quadratic matrix, it can always be transformed into a standard form through orthogonal transformation, with

$$R_{rr} = Q^T \Lambda Q \tag{32}$$

where  $Q$  is the orthogonal matrix of the autocorrelation matrix, which satisfies the following relationship:

$$Q^T Q = I \text{ or } Q^T = Q^{-1} \quad (33)$$

In Equation (32),  $\Lambda$  is a diagonal matrix composed of the eigenvalues of  $R_{rr}$ ,

$$\Lambda = \text{diag}[\lambda_1, \lambda_2, \dots, \lambda_L] \quad (34)$$

making

$$V(n) = W(n) - W_0 \quad (35)$$

Subtracting  $W_0$  from both sides of Equation (29) and using the relationship of Equation (35)

$$V(n+1) = V(n) - \Lambda V(n) \frac{\mu \Gamma(2) |V(n) + W_0|^{1-v}}{\Gamma(2-v)} + \lambda [V(n) - V(n-1)] \quad (36)$$

Converting Equation (36) into a scalar form, the  $l_e^{\text{th}}$  component satisfies

$$v_{l_e}(n+1) = v_{l_e}(n) - \mu \lambda_{l_e} v_{l_e}(n) \frac{\Gamma(2) |v_{l_e}(n) + W_0|^{1-v}}{\Gamma(2-v)} + \lambda [v_{l_e}(n) - v_{l_e}(n-1)]_0 \quad (37)$$

Taking the mathematical expectation on both ends of the equal sign of Equation (37)

$$E[v_{l_e}(n+1)] = E[v_{l_e}(n)] - \mu \lambda_{l_e} E[v_{l_e}(n)] \frac{\Gamma(2) |E[v_{l_e}(n)] + W_0|^{1-v}}{\Gamma(2-v)} + \lambda [E[v_{l_e}(n)] - E[v_{l_e}(n-1)]] \quad (38)$$

In the convergence interval of the algorithm, when  $n \rightarrow \infty$ ,  $E[v_{l_e}(n+1)] = E[v_{l_e}(n)]$ ; thus, Equation (38) can be simplified as

$$\mu \lambda_{l_e} E[v_{l_e}(n)] \frac{\Gamma(2) |E[v_{l_e}(n)] + W_0|^{1-v}}{\Gamma(2-v)} = 0 \quad (39)$$

There are two solutions to Equation (39):  $E[v_{l_e}(\infty)] = 0$  and  $E[v_{l_e}(\infty)] = -W_0$ . The former is that all values of the initial state are zero; the latter is the value of the optimal solution after the operation, proving that the algorithm can converge stably under the assumption that the iteration time tends to infinity.

### 3. Simulation

First, the convergence speed and convergence steady-state comparison experiments of the algorithm are conducted. The experimental objects include four algorithms FxLMS algorithm, N-LMS algorithm of the normalization algorithm variant, classical SVS-LMS algorithm, and MFO-FxLMS algorithm. These algorithms are compared after adjusting them to the best convergence state. The results of the simulation tests are shown in Figure 3.

In the initial convergence state, the convergence speed of the variable convergence step algorithm has a significant advantage over the fixed convergence step algorithm (Figure 3a). The convergence speed of the proposed MFO-FxLMS algorithm is the fastest with minor fluctuations, which indicates that the algorithm is very stable. In the steady-state stage, the steady-state errors of the four algorithms are divided into two levels, SVS-LMS and MFO-FxLMS are the first level with very low errors, while FxLMS and N-LMS are the second level with large errors (Figure 3b). The error of the first level is approximately one order of magnitude smaller than that of the second level, and the steady-state error of the MFO-FxLMS algorithm is extremely low and smooth without significant fluctuations.

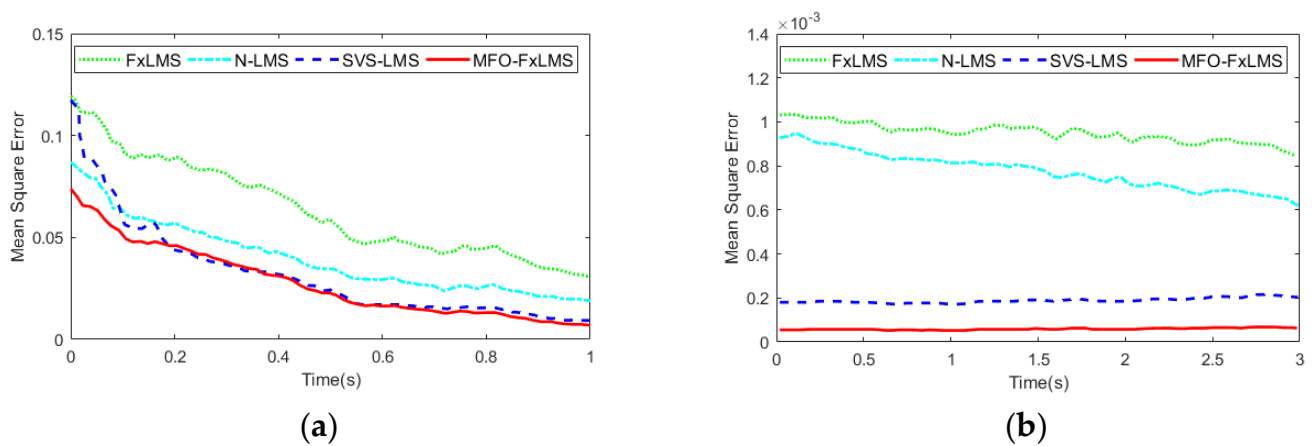


**Figure 3.** Comparison of mean square error of the four algorithms: (a) Early stage of error dynamic convergence; (b) Error convergence steady state.

Two nodes are set in the iterative process of the algorithm. Calculate the number of iterations for each algorithm when the mean square error (MSE) is less than or equal to 0.05 and less than or equal to 0.01 respectively. At the end of the algorithm, the ratio of the current MSE to the initial MSE is calculated and converted into the decay value (dB). The statistics are listed in Table 2.

**Table 2.** Comparative results of the four algorithms.

Algorithm Name	Number of Iterations MSE ≤ 0.05	Number of Iterations MSE ≤ 0.01	Error Attenuation M1 (dB)
FxLMS	665	1527	−33
N-LMS	473	1221	−35
SVS-LMS	408	980	−39
MFO-FxLMS	354	922	−44

From the three statistical data in Table 2, the performance of the four algorithms in descending order is MFO-FxLMS, SVS-LMS, N-LMS, and FxLMS. The performance of the MFO-FxLMS algorithm is greatly improved compared with other common algorithms, and the final steady-state error is reduced by an order of magnitude. The convergence speed is improved by 10–30%, and the steady-state error attenuation is improved by 11 dB, 9 dB and 5 dB respectively compared to FxLMS, N-LMS, and SVS-LMS algorithms, respectively.

A simulation using the proposed multi-channel fractional-order ANC algorithm and the classical FxLMS algorithm were performed with an about 3 × 3 m<sup>2</sup> vehicle noise cancellation target area in MATLAB respectively. In the simulation, the noise sources were a mixture of sinusoidal signals and white noise, and approximately 40 dB of ambient noise was added. The initial convergence step size  $\beta$  in Equation (23) was set to 0.01, and the simulated secondary sound sources were evenly arranged in the area.

The noise cancellation effects of the FxLMS ANC and the fractional-order ANC algorithms (MFO-FxLMS is the fractional-order algorithm in Figure 4) were compared. The results before and after the control are shown in Figure 4a, and the frequency spectrum is shown in Figure 4b. It can be seen that both algorithms can quickly and effectively suppress noise below 1000 Hz, but the fractional-order ANC had a more effective noise reduction process and the noise reduction effect was better than that of the FxLMS ANC algorithm.

Under the same simulation conditions, the number of channels was expanded to multiple channels, and the number of secondary sound sources was the same as the number of channels, evenly distributed in the noise cancellation target area. Extended to multi-channel, the cloud diagrams of sound pressure level over the target area before and after the active noise control are shown in Figure 5a for the case of using the 4-channel fractional-order ANC algorithm.

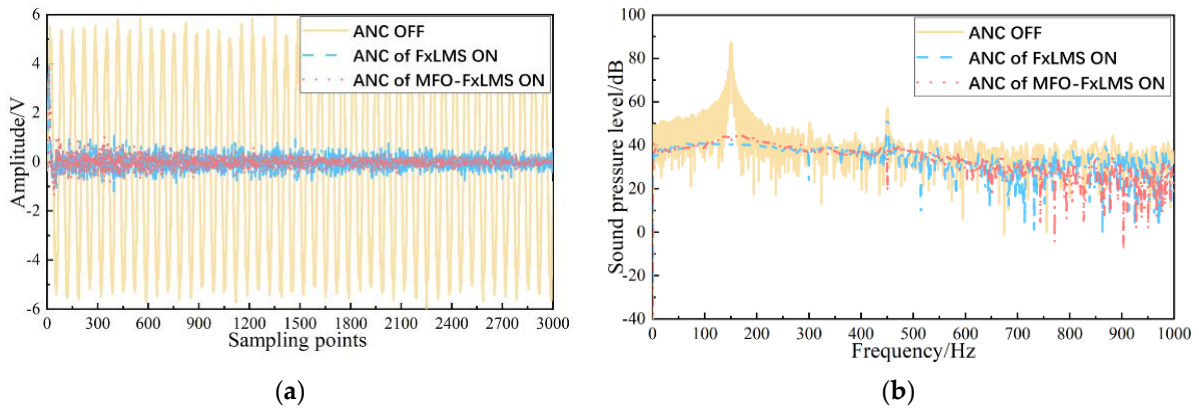


**Figure 4.** Comparison of noise cancellation performance of two algorithms: (a) Time domain diagram; (b) Frequency domain diagram.

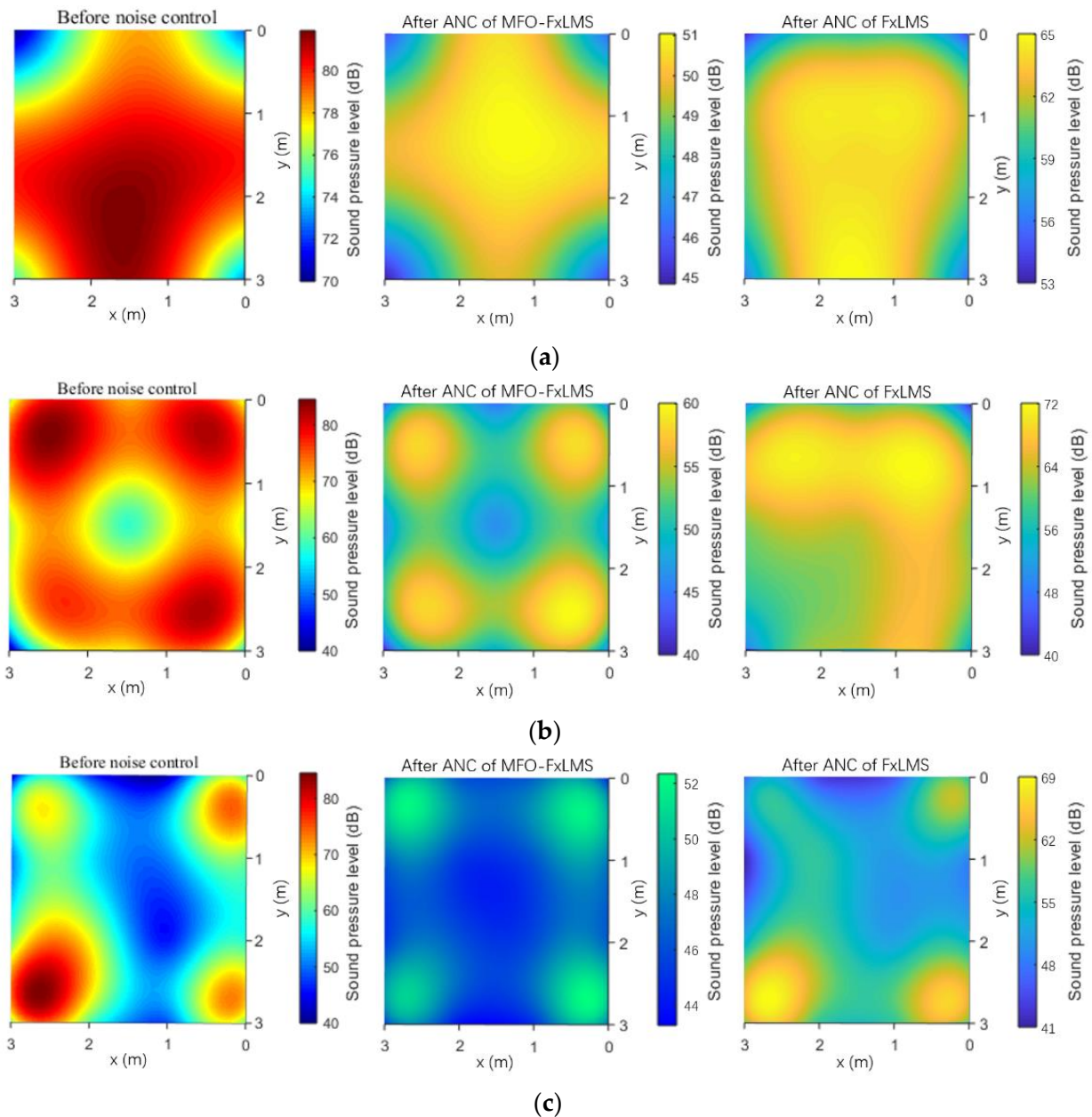


**Figure 5.** Cont.

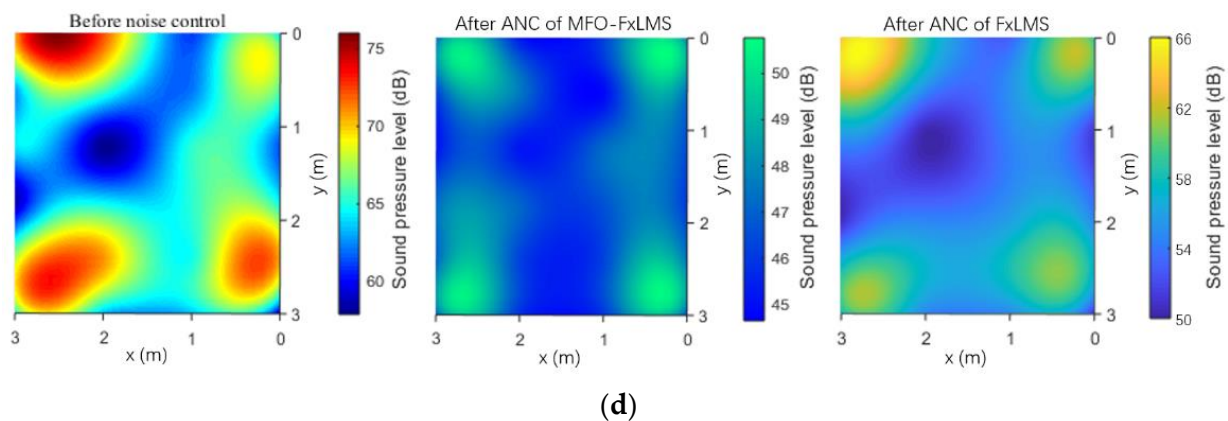


**Figure 5.** Contrast simulation results of MFO-FxLMS and FxLMS algorithms: (a) 4-channel comparison; (b) 8-channel comparison; (c) 16-channel comparison; (d) 24-channel comparison.

According to the information of the color map in Figure 5a, the average noise in this target area was approximately 77 dB, and the highest noise peak was approximately 82 dB. After the noise control of the fractional-order ANC algorithm, the noise in the entire area was significantly reduced, and the average residual noise was approximately 50 dB. In contrast, by the noise control of the FxLMS ANC algorithm, the area of noise reduction was relatively small, the effect of noise reduction was slightly weaker, and the average residual noise was approximately 63 dB. Overall, the noise was reduced by approximately 27 dB through the fractional-order ANC algorithm and 14 dB through the FxLMS ANC algorithm.

In a similar way, fractional-order ANC systems and FxLMS ANC systems with 8, 16, and 24 channels were uniformly arranged in the same size target area space, and the simulation was performed. The results are shown in Figure 5b–d: With the 8-channel ANC system, the noise cancellation coverage was increased; with the 16-channel ANC system, the noise level after noise control was further reduced and became more stable. In the target area, the average noise cancellation after activating the multichannel fractional-order ANC algorithm ranged from 23 to 30 dB. By contrast, the average noise cancellation after activating the FxLMS ANC algorithm was only between 11 dB and 16 dB.

The simulation showed that the multi-channel fractional-order ANC algorithm had a good control effect on the large noise control area. In the same size target area, as the number of channels increased, the noise level in the area was better controlled and distribution was more balanced; as the number of channels decreased, the noise level after control was unevenly distributed, which is relatively stable at the control point, while the noise level changes greatly at the regional boundary.

### 3.1. Experiment

To further verify the effect of the multi-channel fractional-order ANC algorithm under the real scene, we built a vehicle ANC system to control the noise of different frequencies, and further successfully conducted a 4-channel vehicle engine noise cancellation experiment. The experiment was conducted in the anechoic chamber, the background noise inside the anechoic chamber was 20 dB, and the noise cut-off frequency was 50 Hz.

### 3.2. Measurement and Analysis of Vehicle Engine Noise

The experiment involved collecting and analyzing vehicle engine noise in an anechoic chamber. The noise signals were collected using the microphones (Named Mic 1–5 for convenience) and transmitted to the computer for processing. Microphones were arranged in front of, on either side of, and above the vehicle's engine compartment and at the headrest of the vehicles seat (Figure 6). The vehicle was started and ran stably at different speeds, and the signal noise data were recorded in real time. The peak frequency of the vehicle engine noise fluctuated within 20–150 Hz (Figure 7).

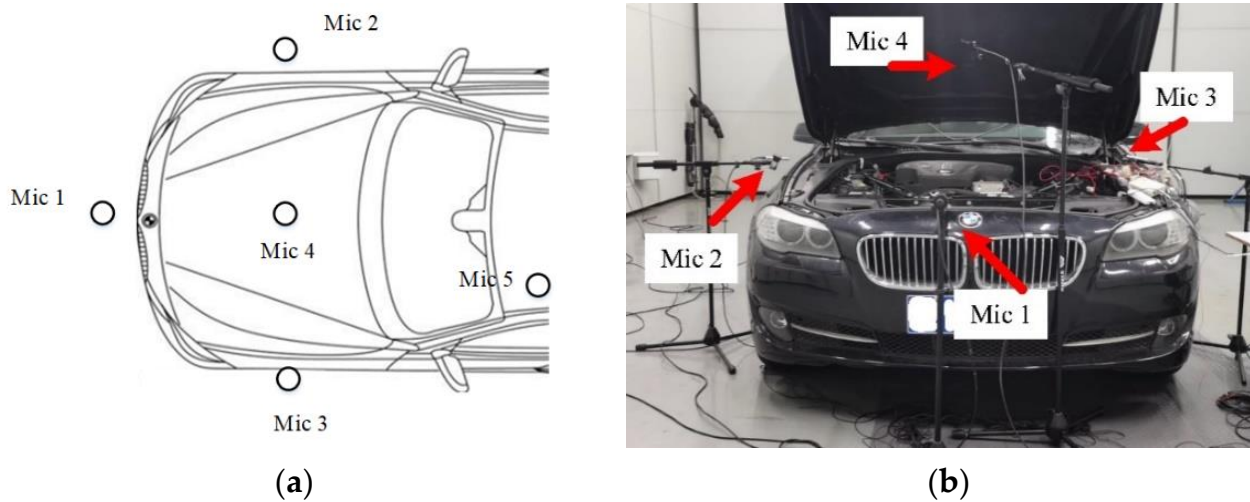


**Figure 6.** Experimental arrangement of vehicle engine noise measurement: (a) Microphone arrangement; (b) Experimental apparatus arrangement.

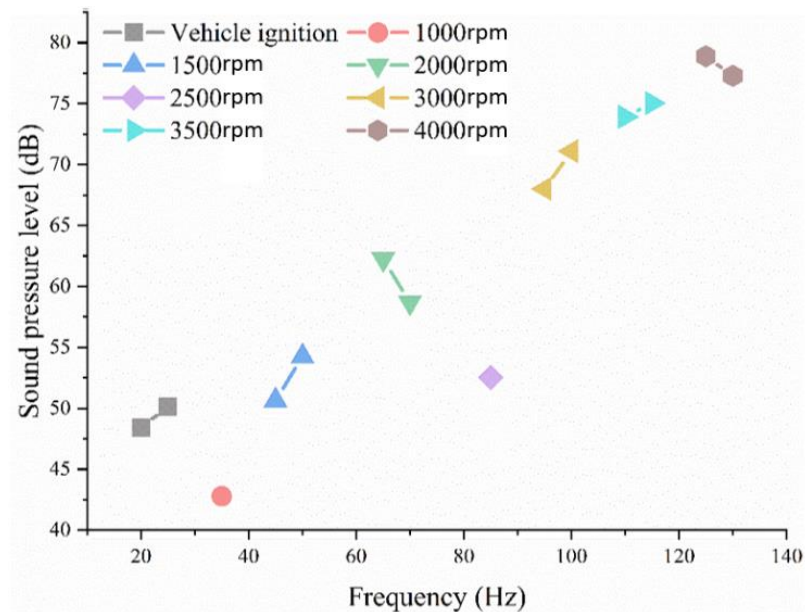


**Figure 7.** Main noise frequency contribution analysis diagram of the vehicle engine.

The measured noise data showed that the noise contribution of the vehicle engine was mainly concentrated within 150 Hz. The noise changed significantly as the speed varied and was positively correlated, and the sound pressure level of the noise increased with the speed. Therefore, aiming at reducing the noise peaks under these working conditions, a multi-channel fractional-order ANC algorithm was used for vehicle engine noise cancellation.

### 3.3. The Vehicle ANC System for Experiment

The architecture of the implemented ANC system based on the floating-point MFO-FxLMS algorithm is shown in Figure 8. Here, National Instruments (NI) Compact-DAQ chassis (cDAQ-9189) was used as the controller and programmed on LABVIEW. The analog input and output modules were formed with NI-9215 and NI-9263 modules. In this controller, length  $L$  of the control filter was set to 50 taps, the initial step size was set to 0.01, the sampling rate was set to 1 kHz, the number of pulses for the secondary path identification was set to 500, and the step size was set to 0.008.

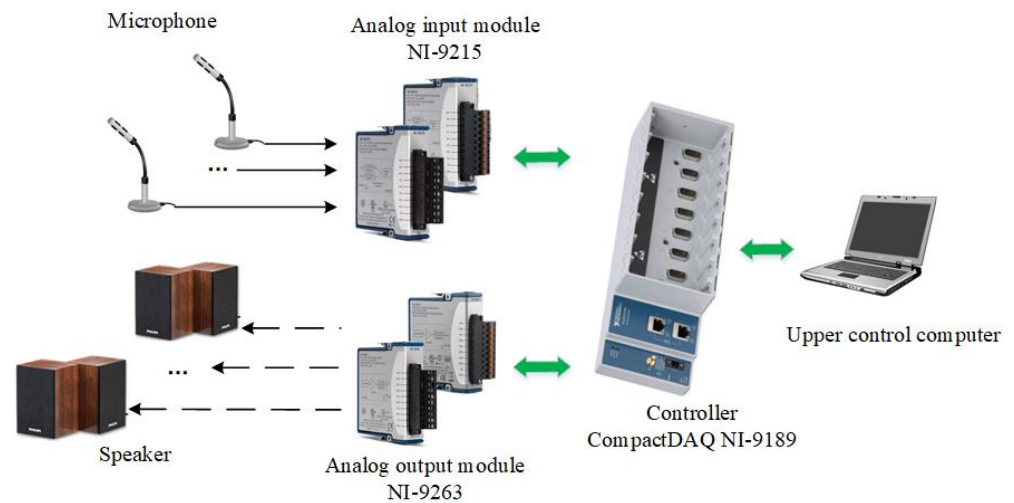
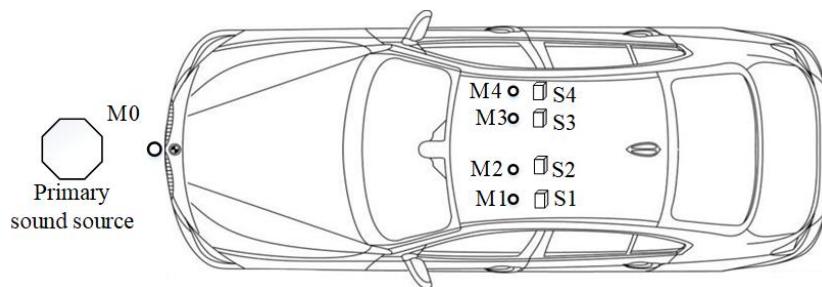


**Figure 8.** Schematic diagram of the composition of the multi-channel fractional-order ANC system.

The experiment layout is shown in Figure 9a. There were four desired signal sensors and one reference signal sensor. The reference sensor was placed in the engine compartment of the vehicle, whereas the desired signal sensors were placed at the four seat headrests. The primary sound source was a high-power omnidirectional loudspeaker placed at approximately 10 cm from the front of the vehicle. A reference microphone was placed at 5 cm from the front of the spherical power amplifier to collect the sound source signal (Figure 9b). The error microphones were placed at four measurement points in the vehicle (M1–M4). To ensure that the distance between each control area and the noise source was consistent and the sound field was similar, an error microphone and secondary sound source speaker were placed 10 cm away from each other at the headrests of the driving and copilot seats (Figure 9c).



(a)



(b)



(c)

**Figure 9.** Vehicle multi-channel fractional-order ANC experimental system. (a) Laboratory equipment deployment; (b) Arrangement of external sound source of noise in anechoic room; (c) Arrangement of internal sensors and speakers in anechoic room.

### 3.4. Noise Cancellation of External Spherical Sound Source of Vehicle

The secondary path was identified and the secondary sound source was achieved by playing white noise. The signals collected by error microphones M1, M2, M3, and M4 were used to identify the secondary path in the driving and copilot positions. The primary sound source was played with noise signals of different frequencies (The frequency is between 80–500 Hz), which were collected by the reference microphone. The error microphone collected the residual noise signals and then transmitted them to the controller for calculations based on the MFO-FxLMS algorithm. The output control signals were obtained and transmitted to the secondary sound source for playback. The signal acquisition instrument monitored the noise at the error microphone in the target area, displaying its sound pressure level and spectrum characteristics in real time through LabVIEW.

The interior space of the vehicle was approximately 2800 mm long and 1700 mm wide, a 4-channel fractional-order ANC algorithm was used for the experiment of the vehicle noise cancellation. According to the vehicle engine noise characteristics, representative noise frequencies were selected for the 4-channel noise test experiments of single- and mixed-frequency noises, respectively. The single frequency noise test was performed at 80, 100, 200, 300, and 400 Hz noise, evenly distributed between 80 and 450 Hz. The mixed-frequency noise test selected three noises at a time, and the three noises were distributed in the intervals of 20–200, 150–350, and 300–500 Hz. The noise data collected before and after the noise cancellation is shown in Table 3.

**Table 3.** 4-channel fractional-order ANC noise cancellation statistics.

Noise Source (Hz)	Before Noise Control M1–M4 (dB)	After Noise Control M1–M4 (dB)	Noise Cancellation M1–M4 (dB)
80	53.42/55.20/54.09/52.13	33.87/33.92/34.60/35.09	19.54/21.28/19.48/17.04
100	53.75/54.82/52.65/48.03	32.19/32.32/30.55/32.63	21.56/22.50/22.11/15.40
200	59.62/57.29/56.76/57.68	32.71/31.49/28.77/32.78	26.91/25.80/27.99/24.90
300	54.02/49.60/45.23/57.15	29.36/32.34/27.24/31.29	24.65/17.25/17.99/25.86
400	58.40/48.26/43.69/56.35	29.71/28.30/27.28/29.23	28.68/19.95/16.41/27.13
100 180 300 (mix)	53.92/57.70/52.11/53.46	40.03/41.92/41.42/37.61	13.90/15.78/10.69/15.85
150 250 400 (mix)	53.89/49.58/7.52/50.95	29.30/29.17/34.73/32.07	24.59/20.41/12.79/18.88
200 350 450 (mix)	51.58/48.76/48.40/50.53	31.73/28.18/26.24/35.00	19.85/20.58/22.15/15.53

Comparing the noise level of the error microphone in the target area under the combined action of the primary and secondary sound sources, the noise source was at a single frequency of 200 Hz and at mixed frequencies of 150, 250, and 400 Hz. The sound pressure level changes are shown in Figure 10. The spectrum of sound pressure level achieved is shown in Figure 11.

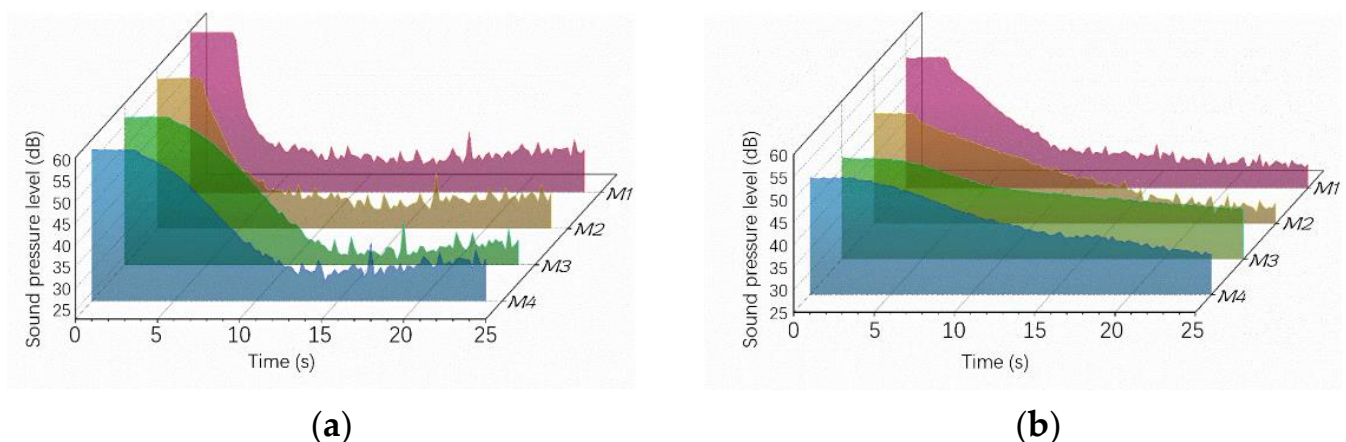


**Figure 10.** Variation curve of the sound pressure level of the noise: (a) 200 Hz single-frequency; (b) 150 Hz, 250 Hz, and 400 Hz mixed-frequency.

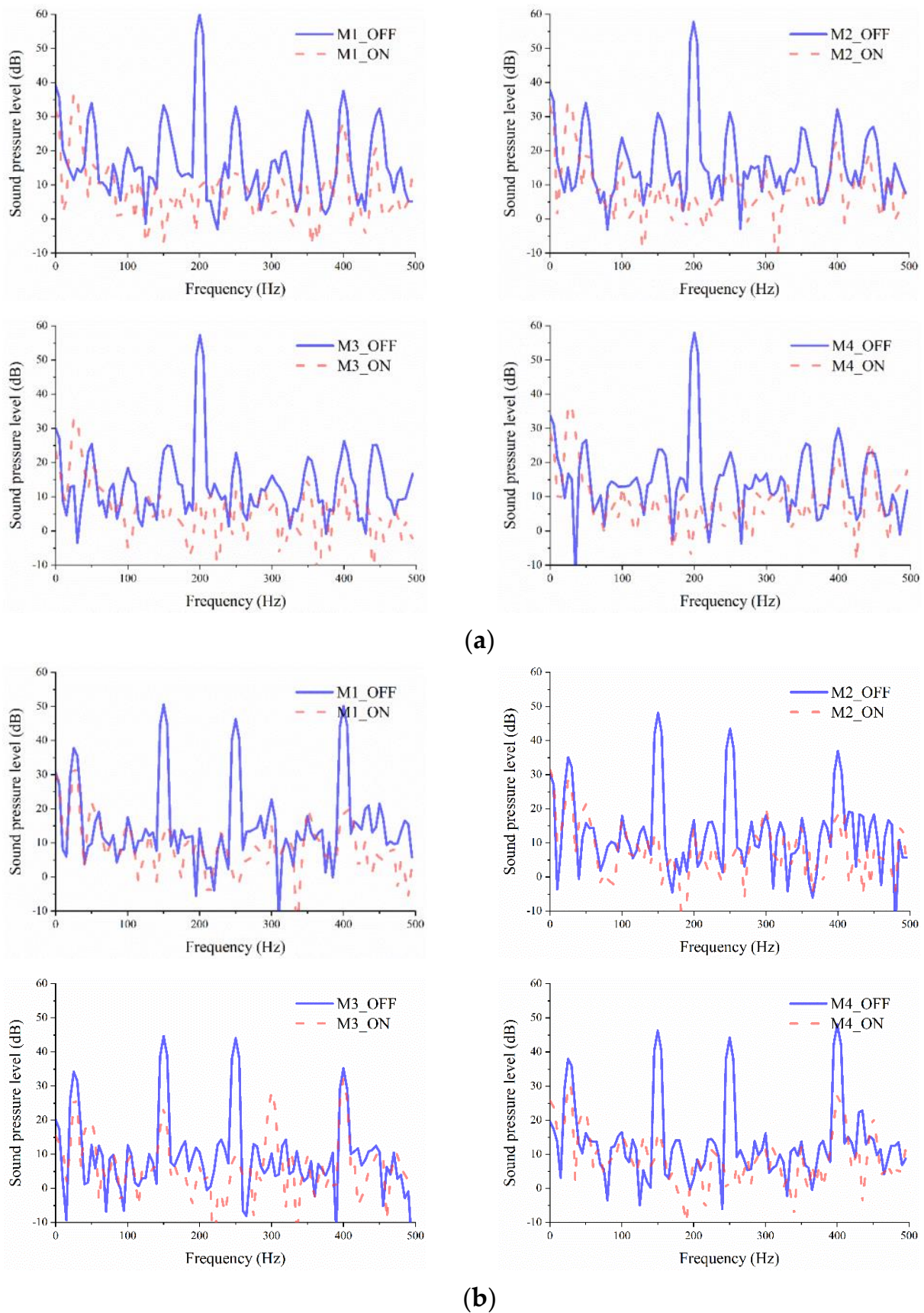


**Figure 11.** Noise spectrum of the target area before and after 4-channel fractional-order active noise control: (a) 200 Hz single-frequency; (b) 150 Hz, 250 Hz, and 400 Hz mixed-frequency.

The experimental results showed that the algorithm led to an average noise cancellation of nearly 22 dB for single-frequency noise below 400 Hz. The highest noise reduction reached 28 dB. The noise cancellation for the mixed frequency noise source was not as great as for the single frequency source because of the increase of the signal complexity, but the average noise cancellation reached 17 dB. After the ANC was turned on, the sound pressure level of the noise was immediately reduced, finally reaching a stable state at approximately 30 dB. The frequency spectrum in Figure 11 shows that the sound pressure level of the noise at the frequency where the noise was the main contribution was greatly reduced after the algorithm was turned on, whereas the sound pressure levels at other frequencies did not show large improvement.

### 3.5. Noise Cancellation of Vehicle Engine Noise

For further testing the proposed vehicle ANC system on the vehicle engine noise cancellation, the reference microphone was placed in the vehicle's engine compartment (see Figure 12).

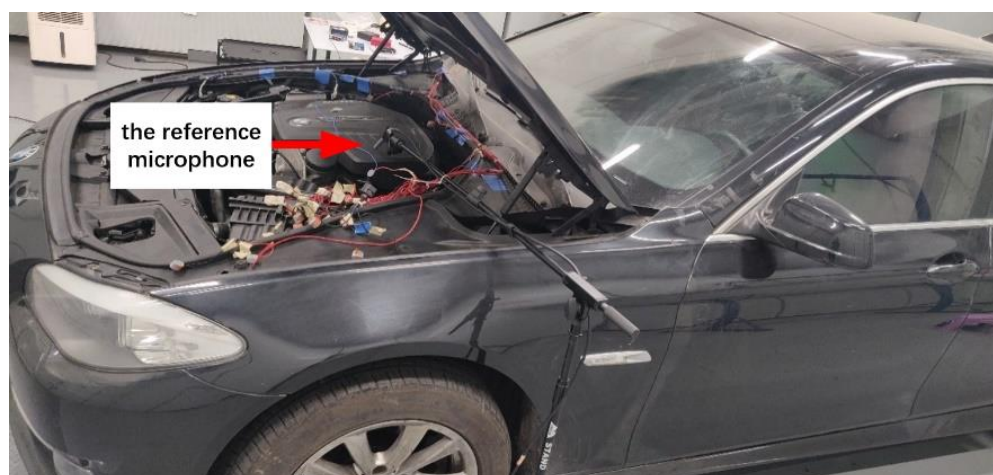


**Figure 12.** Arrangement of the reference sensor.

In terms of the measurement and analysis of the engine noise, along with the change in engine speed, the change range of noise in the engine compartment of the vehicle was mainly concentrated between approximately 50 and 150 Hz. Considering the normal driving speed of the vehicle and the frequency response range of the secondary sound source speakers, the noise at 2500, 3000, and 3500 r/min was actively controlled respectively. The vehicle was tested at different engine speeds and the multi-channel fractional-order ANC algorithm was applied. The results of the noise cancellation before and after ANC are shown in Table 4. The spectrogram before and after the 4-channel noise control is shown in Figure 13.

**Table 4.** 4-channel fractional-order ANC algorithm vehicle engine noise control data statistics.

Rotation Speed (r/min)	Before Noise Control M1–M4 (dB)	After Noise Control M1–M4 (dB)	Noise Cancellation M1–M4 (dB)
2500	52.99/52.35/52.23/52.19	49.25/47.83/47.11/48.58	3.74/4.52/5.12/3.61
3000	52.99/52.35/52.23/52.19	49.33/48.17/45.32/47.11	3.66/4.18/6.91/5.08
3500	53.18/51.01/50.06/51.86	46.14/46.31/47.41/46.90	7.04/4.70/2.65/4.96

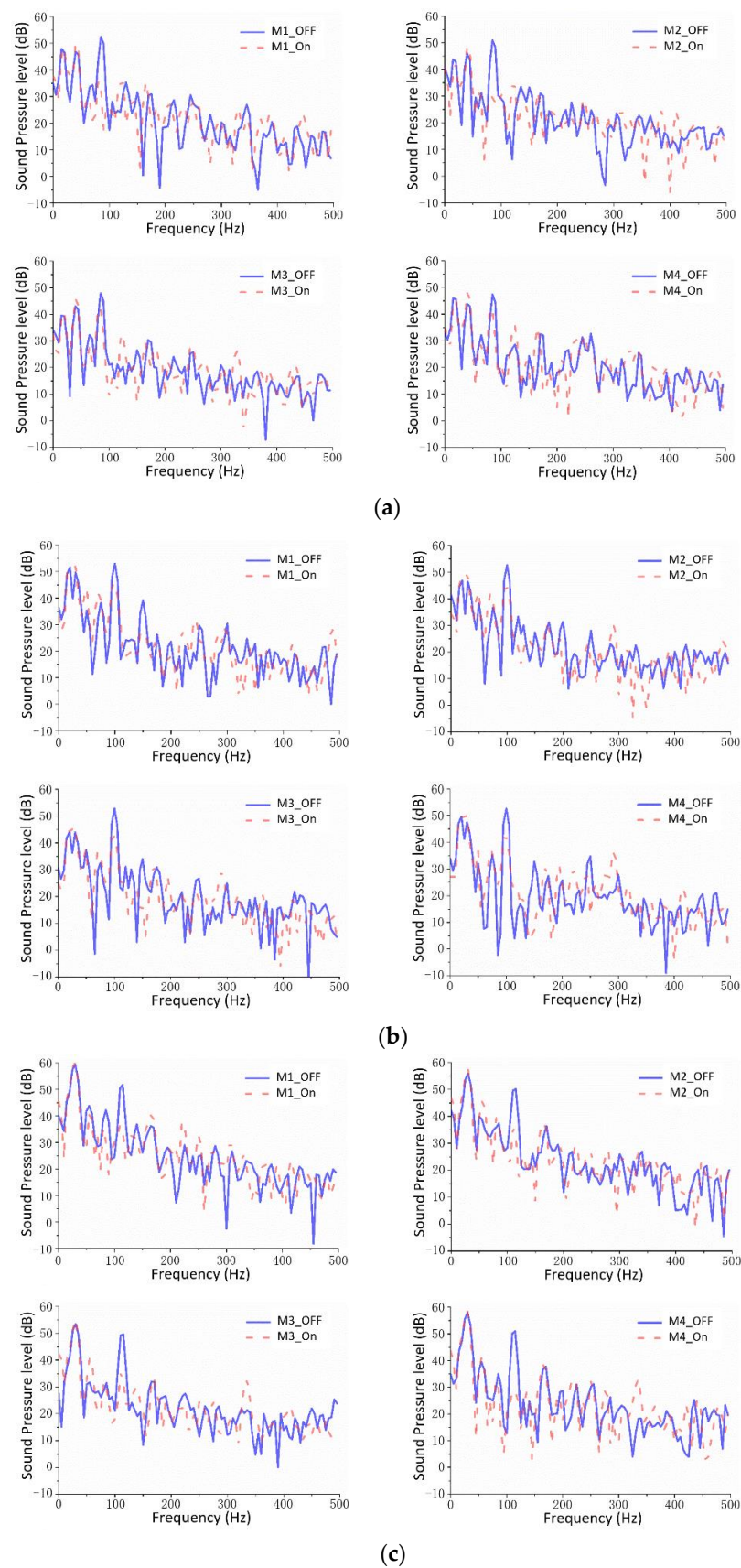


**Figure 13.** Noise spectrum diagrams before and after noise control of vehicle engine noise at different speeds: (a) Spectrum before and after active noise control (ANC) at 2500 r/min; (b) Spectrum before and after ANC at 3000 r/min; (c) spectrum before and after ANC at 3500 r/min.

As shown in Figure 13, because the vehicle engine noise changed with the speed, corresponding to a certain frequency, after the multi-channel fractional-order ANC algorithm was turned on, the amplitude at the peak frequency of the engine noise was significantly reduced by more than 10 dB, and the total noise cancellation was reduced by approximately 4.7 dB on average (Table 4). Most of the noise below 50 Hz was generated by the resonance of the vehicle body structure and should be optimized from the perspective of vibration reduction. Overall, it was demonstrated that the multi-channel fractional-order ANC algorithm is capable of effectively reducing the engine noise in the target area and expanding the silent zone.

#### 4. Conclusions

The multi-channel fractional-order ANC algorithm was proposed in this study with the use of fractional-order calculus, multiple input and output feedback, and variable time steps for convergence. The experimental results showed that the proposed algorithm is suitable for the cancellation of vehicle engine noise with a large control area. The following are the conclusions of this study:

1. The simulation of the fractional-order ANC algorithm proved that the fractional calculus, as a replacement to the integer gradient drop to update the filter weightings, improves the accuracy of the algorithm. The resulting residual noise obtained using the proposed algorithm is smaller than using the conventional FxLMS algorithm.
2. The proposed algorithm simulations show that when the number of speakers was enough to reflect all noise activities in the control area, the area noise was reduced to a relatively low and stable level. In the same size control area, as the number of channels increases, the noise level in the area is better controlled than the conventional FxLMS algorithm and the acoustical distribution is more balanced. With the number of channels decreased, the noise level after control is unevenly distributed, which is relatively stable near the control point, while the noise level changes greatly at the boundary of the region.
3. The experimental results in reducing the noise of the spherical sound source outside the vehicle show that for single-frequency external noise sources below 400 Hz, the proposed algorithm successfully reduced the noise by approximately 22 dB on average, whereas for mixed-frequency external noise, the average noise reduction reached 17 dB.
4. The proposed algorithm can effectively control the low-frequency noise of vehicle engines mainly in the frequency range of 50–150 Hz. At the peak frequency, the noise was reduced by approximately 10 dB, and the total noise cancellation was approximately 4.7 dB on average.

**Author Contributions:** Conceptualization, T.L.; methodology, T.L. and N.W.; software, M.W. and Y.H.; validation, M.W., Y.H., and N.W.; formal analysis, J.Y.; data curation, M.W.; writing—original draft preparation, N.W.; writing—review and editing, Y.H.; visualization, J.Y.; supervision, R.D.; project administration, K.Z. All authors have read and agreed to the published version of the manuscript.

**Funding:** This work was supported by the Natural Science Foundation of Hunan Province under Grant 2020JJ6067.

**Conflicts of Interest:** The authors declare no conflict of interest.

#### References

1. Elliott, S.J.; Nelson, P.A. Active noise control. *Signal Processing Mag.* **1993**, *10*, 12–35. [[CrossRef](#)]
2. Kuo, S.M.; Morgan, D.R. Active noise control: A tutorial review. *Proc. IEEE* **1999**, *87*, 943–973. [[CrossRef](#)]
3. Kuo, S.M.; Morgan, D.R. *Active Noise Control Systems: Algorithms and DSP Implementations*; John Wiley & Sons: New York, NY, USA, 1996.
4. Patel, V.; Cheer, J.; Fontana, S. Design and Implementation of an Active Noise Control Headphone with Directional Hear-Through Capability. *IEEE Trans. Consum. Electron.* **2020**, *66*, 32–40. [[CrossRef](#)]

5. Chang, H.-Y.; Luo, C.-H.; Lo, T.-S.; Tai, C.-C. Compensated active noise cancellation earphone for audiometric screening tests in noisy environments. *Int. J. Audiol.* **2019**, *58*, 747–753. [[CrossRef](#)] [[PubMed](#)]
6. Zhang, S.; Wang, Y.; Guo, H.; Yang, C.; Wang, X.; Liu, N. A normalized frequency-domain block filtered-x LMS algorithm for active vehicle interior noise control. *Mech. Syst. Signal Process.* **2019**, *120*, 150–165. [[CrossRef](#)]
7. Arena, M.; Fenza, A.D.; Giulio, M.D.; Paonessa, A.; Amoroso, F. Progress in studying passive and active devices for fuselage noise reduction for next generation turboprop. *Ceas Aeronaut. J.* **2017**, *8*, 302–312. [[CrossRef](#)]
8. Sahib, M.A.; Streif, S. Design of an active noise controller for reduction of tire/road interaction noise in environmentally friendly vehicles. In *2017 Signal Processing: Algorithms, Architectures, Arrangements, and Applications (SPA)*; IEEE: Piscataway, NJ, USA, 2017; pp. 59–62.
9. Sachau, D.; Jukkert, S.; Hövelmann, N. Development and experimental verification of a robust active noise control system for a diesel engine in submarines. *J. Sound Vib.* **2016**, *375*, 1–18. [[CrossRef](#)]
10. Wang, W.; Thomas, P. Low-frequency active noise control of an underwater large-scale structure with distributed giant magnetostrictive actuators. *Sensors Actuators A Phys.* **2017**, *263*, 113–121. [[CrossRef](#)]
11. Zhao, T.; Liang, J.; Zou, L.; Zhang, L. A New FXLMS Algorithm with Offline and Online Secondary-Path Modeling Scheme for Active Noise Control of Power Transformers. *IEEE Trans. Ind. Electron.* **2017**, *64*, 6432–6442. [[CrossRef](#)]
12. Li, Z.; Li, D.; Xu, X.; Zhang, J.Q. New normalized LMS adaptive filter with a variable regularization factor. *J. Syst. Eng. Electron.* **2019**, *30*, 41–51.
13. Jingfan, Q.; Jingzheng, O.Y. A New Variable Step Size LMS Adaptive Filtering Algorithm. *Data Collect. Process.* **1997**, *3*, 171–174.
14. Elliott, S.J.; Cheer, J. Modeling local active sound control with remote sensors in spatially random pressure fields. *J. Acoust. Soc. Am.* **2015**, *137*, 1936–1946. [[CrossRef](#)] [[PubMed](#)]
15. Cheer, J.; Daley, S. An Investigation of Delayless Subband Adaptive Filtering for Multi-Input Multi-Output Active Noise Control Applications. *IEEE/ACM Trans. Audio Speech Lang. Process.* **2017**, *25*, 359–373. [[CrossRef](#)]
16. Lorente, J.; Ferrer, M.; de Diego, M.; Gonzalez, A. The frequency partitioned block modified filtered-x NLMS with orthogonal correction factors for multichannel Active Noise Control. *Digit. Signal Process.* **2015**, *43*, 47–58. [[CrossRef](#)]
17. Zhang, J.; Abhayapala, T.D.; Samarasinghe, P.N.; Zhang, W.; Jiang, S. Multichannel active noise control for spatially sparse noise fields. *J. Acoust. Soc. Am.* **2016**, *40*, EL510. [[CrossRef](#)]
18. Patel, V.; George, N. Multi-channel spline adaptive filters for non-linear active noise control. *Appl. Acoust.* **2019**, *161*, 107142. [[CrossRef](#)]
19. Lopes, P.A.C.; Gerald, J.A.B.; Piedade, M.S. The Random Walk Model Kalman Filter in Multichannel Active Noise Control. *IEEE Signal Process. Lett.* **2015**, *22*, 2244–2248. [[CrossRef](#)]
20. Yu, Y.; Zhao, H. Performance analysis of the deficient length NSAF algorithm and a variable step size method for improving its performance. *Digit. Signal Process.* **2017**, *62*, 157–167. [[CrossRef](#)]
21. Huang, F.; Zhang, J.; Zhang, S. Combined-Step-Size Affine Projection Sign Algorithm for Robust Adaptive Filtering in Impulsive Interference Environments. *IEEE Trans. Circuits Syst. II Express Briefs* **2016**, *63*, 493–497. [[CrossRef](#)]
22. Huang, F.; Zhang, J.; Zhang, S. Combined-Step-Size Normalized Subband Adaptive Filter with a Variable-Parametric Step-Size Scaler Against Impulsive Interferences. *IEEE Trans. Circuits Syst. II Express Briefs* **2018**, *65*, 1803–1807. [[CrossRef](#)]
23. Lara, P.; Igreja, F.; Tarrataca, L.D.T.J.; Haddad, D.B.; Petraglia, M.R. Exact Expectation Evaluation and Design of Variable Step-Size Adaptive Algorithms. *IEEE Signal Process. Lett.* **2019**, *26*, 74–78. [[CrossRef](#)]
24. Jahromi, M.N.S.; Salman, M.S.; Hocanin, A.; Kukrer, O. Convergence analysis of the zero-attracting variable step-size LMS algorithm for sparse system identification. *Signal Image Video Process* **2015**, *9*, 1353–1356. [[CrossRef](#)]
25. Shi, L.; Zhao, H. Variable step-size distributed incremental normalised LMS algorithm. *Electron. Lett.* **2016**, *52*, 519–521. [[CrossRef](#)]
26. West, B.J.; Bologna, M.; Grigolini, P. *Physics of Fractal Operators*; Springer: New York, NY, USA, 2013.
27. Zhang, X.; Wu, J.; Liu, L.; Wu, Y.; Cui, Y. Convergence analysis of iterative scheme and error estimation of positive solution for a fractional differential equation. *Math. Model. Anal.* **2018**, *23*, 611–626. [[CrossRef](#)]
28. Li, Y.-X.; Yang, G.-H. Observer-Based Fuzzy Adaptive Event-Triggered Control Codesign for a Class of Uncertain Nonlinear Systems. *IEEE Trans. Fuzzy Syst.* **2018**, *26*, 1589–1599. [[CrossRef](#)]
29. Wang, X.; Ouannas, A.; Pham, V.-T.; Abdolmohammadi, H.R. A fractional-order form of a system with stable equilibria and its synchronization. *Adv. Differ. Equations* **2018**, *2018*, 20. [[CrossRef](#)]
30. Duarte-Mermoud, M.A.; Aguila-Camacho, N.; Gallegos, J.A.; Castro-Linares, R. Using general quadratic Lyapunov functions to prove Lyapunov uniform stability for fractional order systems. *Commun. Nonlinear Sci. Numer. Simul.* **2015**, *22*, 650–659. [[CrossRef](#)]
31. Ba, H.B.; Cao, J.D. Projective synchronization of fractional-order memristor-based neural networks. *Neural Networks* **2015**, *63*, 1–9. [[CrossRef](#)]
32. Wang, C.; Liang, M. Adaptive Backstepping Control of a Class of Incommensurate Fractional Order Nonlinear MIMO Systems with Unknown Disturbance. *IEEE Access* **2019**, *7*, 150949–150959. [[CrossRef](#)]
33. Wang, C.; Liang, M.; Chai, Y. Adaptive Control of a Class of Incommensurate Fractional Order Nonlinear Systems with Input Dead-Zone. *IEEE Access* **2019**, *7*, 153710–153723. [[CrossRef](#)]
34. Gong, P.; Lan, W. Adaptive Robust Tracking Control for Multiple Unknown Fractional-Order Nonlinear Systems. *IEEE Trans. Cybern.* **2019**, *49*, 1365–1376. [[CrossRef](#)] [[PubMed](#)]

35. Pu, Y.-F.; Zhou, J.-L.; Zhang, Y.; Zhang, N.; Huang, G.; Siarry, P. Fractional Extreme Value Adaptive Training Method: Fractional Steepest Descent Approach. *IEEE Trans. Neural Netw. Learn. Syst.* **2017**, *26*, 653–662. [[CrossRef](#)] [[PubMed](#)]
36. Aslam, M.S.; Raja, M.A.Z. A new adaptive strategy to improve online secondary path modeling in active noise control systems using fractional signal processing approach. *Signal Process.* **2015**, *107*, 433–443. [[CrossRef](#)]
37. Shah, S.; Samar, R.; Raja, M.; Chambers, J. Fractional normalised filtered-error least mean squares algorithm for application in active noise control systems. *Electron. Lett.* **2014**, *50*, 973–975. [[CrossRef](#)]
38. Akhtar, M.T.; Raja, A.Z. Fractional processing-based active noise control algorithm for impulsive noise. In Proceedings of the IEEE China Summit & International Conference on Signal & Information Processing IEEE, Chengdu, China, 12–15 July 2015.
39. Tahir Akhtar, M. Fractional lower order moment based adaptive algorithms for active noise control of impulsive noise sources. *J. Acoust. Soc. Am.* **2012**, *132*, 456–462. [[CrossRef](#)]
40. Liu, L.; Pottim, K.R.; Kuo, S.M. Ear Field Adaptive Noise Control for Snoring: An Real-time Experimental Approach. *IEEE/CAA J. Autom. Sin.* **2019**, *6*, 158–166. [[CrossRef](#)]
41. Jeripotula, P.R.; Kumar, C.A.; Naik, B.R. A novel sign variable step size LMS (SiVSS-LMS) algorithm for adaptive beamforming. *CSI Trans. ICT* **2020**, *8*, 377–384. [[CrossRef](#)]
42. Liu, L.; Li, Y.; Kuo, S.M. Feed-forward active noise control system using microphone array. *IEEE/CAA J. Autom. Sin.* **2018**, *5*, 946–952. [[CrossRef](#)]
43. Patnaik, A.; Nanda, S. The variable step-size LMS/F algorithm using nonparametric method for adaptive system identification. *Int. J. Adapt. Control. Signal Process.* **2020**, *34*, 1799–1811. [[CrossRef](#)]